Role of the N-Terminal Helix I for Dimerization and Stability of the Calcium-Binding Protein S100B

Peter L. Ferguson and Gary S. Shaw*

Department of Biochemistry and R. S. McLaughlin Macromolecular Structure Facility, The University of Western Ontario, London, Ontario N6A 5C1, Canada

Received September 17, 2001; Revised Manuscript Received November 13, 2001

ABSTRACT: Human S100B($\beta\beta$) is a small intracellular EF-hand calcium-binding protein that consists of two noncovalently associated 91-residue β monomers. The three-dimensional structures of S100B reveal the dimer interface consists of four α-helices (I, I′ and IV, IV′) packed in an X-type bundle. In this study, guanidine hydrochloride denaturation and dynamic light scattering were used to assess the impact of single (L3A, L3S, M7A, I11A, F14A) and double (L3A/I11A and L3A/F14A) substitution mutations in helix I on the stability and dimerization propensity of S100B. The free energy of unfolding (ΔG_u) of wild-type apo-S100B was determined to be 72.4 ± 4.0 kJ mol^{-1}, consistent with it being the most stable calcium-binding protein to date. The order of stability of the mutants in their apo form is S100B > L3A > L3S > I11A > M7A ∼ L3A/I11A > F14A > L3A/F14A. Further, there is a strong correlation between the stability and the cooperativity of unfolding. Each mutation proved to be more stable in its calcium form compared to its apo form. The calcium-bound L3S substitution proved to be significantly more stable than calcium-saturated S100B, whereas the L3A, I11A, and L3A/I11A mutants are only slightly more stable than the wild-type protein. The F14A and L3A/F14A mutants are significantly reduced in stability, even in the presence of calcium.

A large number of proteins bind calcium via pairs of the helix−loop−helix motif called the EF-hand (*1*−*4*). Like the well-studied examples of calmodulin, parvalbumin, and troponin C, many of the EF-hand calcium-binding proteins act as intracellular signal transducers by responding to changes in calcium ion concentrations within the cell. The calcium-activated forms of these signaling proteins bind to target proteins to effect changes in cell growth, metabolism, and motility. Human S100B($\beta\beta$) is a small intracellular EF-hand calcium-binding protein found primarily in glial cells. It consists of two noncovalently associated 91-residue β monomers. The best-characterized biological role of S100B is as a calcium-dependent modulator of cytoskeletal assembly and function (*4*). S100B has been implicated in causing or exascerbating the symptoms of Alzheimer's disease (*5*−*8*). In particular, the formation of the neuritic plaques (neurofibrillary tangles of hyperphosphorylated tau protein) characteristic of the disease is intriguing since the phosphorylation of tau can be regulated in a calcium-dependent manner by S100B (*8*).

S100B is a member of the S100 protein family. The 19 members of this family are small (9−13 kDa), acidic, and strongly conserved among vertebrates, and each is usually restricted to one or a few tissue types (*2*−*4*). Two features of the S100 protein family set them apart from most other EF-hand proteins. First, the two EF-hands within each S100 monomer differ in their conserved sequence and mechanisms of calcium coordination. The loop of the "noncanonical" N-terminal EF-hand is composed of 14 amino acids, is basic, and coordinates calcium by main chain carbonyls, except for the bidentate side chain of the loop's last residue, glutamate. The calcium affinity of this EF-hand is about 5−10-fold lower than that of the C-terminal EF-hand (*9*), whose acidic, 12 amino acid loop more closely resembles the canonical EF-hand in both structure and mechanism of calcium coordination via side chain carbonyls. In common with the other EF-hand proteins, the two EF-hands in S100 proteins function as a pair, sharing a three-residue antiparallel β-sheet. The second distinctive feature of the S100 family is that most of these proteins interact strongly with each other to form homodimers and, in some cases, heterodimers. One exception is the small (75-residue) monomeric protein calbindin D_{9k}, which acts as a calcium buffering protein rather than as a signaling protein. Another is the frog protein p26olf, in which dimerization has been replaced by the dimer-like packing of two covalently linked S100 protein-like domains, resulting from a gene duplication event (*10*, *11*).

The role of dimerization in the function of the S100 proteins is not yet clear, but two nonmutually exclusive hypotheses have been offered. The first is that dimerization produces a pair of target binding sites (rather than only one) that are exposed in the calcium-bound form of the S100 protein. A pair of binding sites in S100B allows the protein to modulate the activity of its target proteins, which themselves are typically dimers (annexin VI) or tetramers (p53) or are in equilibrium between soluble dimers and polymers of indeterminate length (tau, GFAP, tubulin). The ability of some S100 proteins to form heterodimers may help

* To whom correspondence should be addressed. Phone: 519-661-4021. Fax: 519-661-3175. E-mail: shaw@serena.biochem.uwo.ca.

10.1021/bi0118052 CCC: $22.00
Published on Web 02/22/2002

to extend the range of target proteins. The second explanation for the role of dimerization in S100 protein function is that it may modulate calcium affinity. This is exemplified by the 1000-fold stronger calcium affinity for the monomeric protein calbindin D_{9k} ($K_D \sim 10$ nM) compared to S100B ($K_D \sim 10-100$ μM). It has been demonstrated that the packing of the hydrophobic core and the composition, length, and angle between the helices flanking the calcium-binding loop have profound effects on calcium affinity (*12*, *13*). In S100 proteins the dimerization scaffold is mediated by helices I and IV of each monomer, the entering and exiting helices of the two calcium-binding sites. Thus, the helices involved in the dimerization of the S100 proteins may themselves lead to modified calcium affinity due to their helix packing arrangement.

Recently, three-dimensional structures of several S100 proteins (*14*−*22*) have allowed the dimer-forming helices to be identified. However, there have been no attempts to identify the most critical residues and their energetic contributions toward formation of the dimer interface. Here we report the thermodynamic stability of several mutant forms of S100B designed to address the importance of helix I toward dimer formation and calcium affinity.

MATERIALS AND METHODS

Construction of Mutants. Mutations in helix I of human S100B were constructed by PCR-based mutagenesis (*23*). S100B DNA from bacterial expression plasmid pSS2 (*24*) was used as a PCR template for the single mutants, whereas pSS2-L3A was the PCR template for construction of the L3A/I11A and L3A/F14A double mutants using the I11A and F14A forward primers. The PCR reverse primer was 5′-CCTAGATCTTCATGTTCAAAGAACTCGTGGCAGGC-3′ in all cases. Forward primers were L3A (5′-CAGAATTCTGGAGGATTTTAAAATGTCTGAGGCTGAGAGG-3′), L3S (5′-CAGAATTCTGGAGGATTTTAAAATGTCTGAGTCTGAGAAGG-3′), M7A (5′-AGAATTCTGGAGGATTTTAAAATGTCTGAGCTGGAGAAGGCCGCTGTGGCCCTCATTGATGTCTTCCAT-3′), I11A (5′-GAAGGCCATGGTGGCCCTCGCTGATGTCTTCCA T-3′), and F14A (5′-GAAGGCCATGGTTGCCCTCATTGATGTCGCTCATCAGTATTCAG-3). The PCR products were inserted into pSS2 using standard molecular cloning techniques. The sequences of the entire coding regions of the reconstructed S100B mutants were confirmed by DNA sequencing at the Robarts Research Institute (London, Ontario).

Protein Expression and Purification. Wild-type S100B and the mutated proteins were expressed and purified from *Escherichia coli* strain N99, as described previously (*24*). All proteins judged to be greater than 99% pure, based on SDS−PAGE, were confirmed and further characterized by mass spectrometry (UWO Biological Mass Spectrometry Laboratory).

Analytical Ultracentrifugation. Purified protein samples were dialyzed into 50 mM Tris-HCl (pH 7.2), 50 mM KCl, 1 mM EDTA, and 1 mM DTT. Sedimentation equilibrium studies were performed in a Beckman Model Optima XL-A analytical ultracentrifuge using six-sector Epon charcoal centerpieces in an AN-60 rotor. A variety of protein concentrations, rotor speeds, and temperatures were assayed. Samples were allowed to equilibrate for 18−24 h at the desired speed and temperature before scanning. Averaged absorbance measurements of 30 or 40 scans were taken in 0.002 cm radial steps at wavelength 280 nm ($\epsilon = 3400$ M^{-1} cm^{-1}). The partial specific volumes of the proteins were calculated from amino acid composition data (*25*). The apparent molecular weights of L3A and L3S were calculated using programs supplied by Beckman.

Dynamic Light Scattering. The apo protein preparations in 10 mM MOPS (pH 7.2), 50 mM KCl, 1 mM EDTA, and 1 mM DTT were analyzed in a Protein Solutions (Charlottesville, VA) DynaPro fixed angle photometer to determine their mass and hence oligomeric status.

Circular Dichroism Spectroscopy. Chemical denaturation studies were performed using a Jasco J-810 spectropolarimeter and following previously described methods (*26*). For each GuHCl[1] concentration, the spectra from five scans (250−200 nm) recorded at 20−25 °C in a 1 mm path-length cell were averaged, and the buffer background was subtracted. Individual stock solutions of all proteins were assayed in both their apo and calcium-bound forms. The apo proteins were prepared in 10 mM MOPS (pH 7.2), 50 mM KCl, 1 mM EDTA, and 1 mM DTT. The calcium-bound proteins were in the same buffer except 20 mM $CaCl_2$ was substituted for the 1 mM EDTA. Denaturation of each construct was measured for at least two different protein concentrations differing by 5-fold. The final concentrations ranged from 2.2 to 26 μM with respect to protein dimer. Protein concentrations were determined by using the peak volumes for alanine and leucine from triplicate amino acid analyses performed at the Alberta Peptide Institute.

Initial determination of the denaturation of each protein was made by overnight incubation in the presence of a series of concentrations of GuHCl ranging from 0 to 7.5 M in 0.25 M increments. Stock solutions of 0 and 8 M GuHCl solutions were prepared in 10 mM MOPS (pH 7.2), 50 mM KCl, and either 1 mM EDTA or 20 mM $CaCl_2$. Fresh DTT was added to a final concentration of 1 mM prior to incubation. The 0.25 M increment series allowed determination of the θ_{max} and θ_{min} values that were used to calculate a linear region of denaturation for each protein, which lies approximately between the intervals of 20% and 80% unfolding of the protein (*26*). To better sample the linear region of denaturation of each protein, a second GuHCl series of 0.1 M increments was constructed, either by adding fresh protein to the newly prepared GuHCl series or by appropriate mixing of protein samples from the 0.25 M increment series. In the latter case fresh DTT was also added. Both methods gave similar results.

Data Analysis. Unfolding data obtained from CD experiments were analyzed using the program KaleidaGraph (Synergy Software) for Macintosh using the two-state approach for dimeric proteins (*27*, *28*). Baselines prior to (Y_F) and following (Y_U) the unfolding transition were fitted according to

$$Y_F = k_F[D] + b_F \quad (1a)$$

$$Y_U = k_U[D] + b_U \quad (1b)$$

where [D] is the GuHCl concentration, k_F and k_U are the slopes, and b_F and b_U are the intercepts. The fraction of unfolded protein (F_{app}) was determined according to eq 2

based on the two-state unfolding model described in the Results section.

$$F_{app} = \frac{Y_O - Y_N}{Y_U - Y_N} \quad (2)$$

The observed CD signal at 222 nm (Y_O) for each GuHCl concentration was fit to eq 3 (*27*), which describes unfolding of the total concentration of dimeric protein P_t, in terms of ΔG_u, the free energy of unfolding, m_D, the dependence of ΔG_u on the denaturant concentration, and the above parameters.

$$Y_O = \frac{(Y_U + k_u[D]) - (Y_N + k_N[D])}{4P_t} \times \left[\left[\frac{\exp(-\Delta G_u - m_0[D])}{RT}\right]^2 + 8\left[\frac{\exp(-\Delta G_u - m_0[D])}{RT}\right][P_t]\right]^{1/2} - \left[\frac{\exp(-\Delta G_u - m_0[D])}{RT}\right] + Y_N + k_N \quad (3)$$

RESULTS

Design of Mutations to Human S100B. Three-dimensional structures of a variety of S100 proteins are available from NMR and X-ray crystallographic studies (*14*−*22*). The structures show significant similarity at the dimer interface, which is comprised of helices I, I′ and IV, IV′ (Figure 1). Representative of the S100 structures, helices I and I′ cross at an angle of 142° ± 3° in human Ca^{2+}-S100B, whereas helices IV and IV′ are more nearly antiparallel with an interhelical angle of 155° ± 2° (*14*). Inspection of the structure of Ca^{2+}-S100B shows that K5-A6 and A6′-K5′ are at the bisection of helices I and I′. About 56% of the side chain area of each A6 is buried at the interface. Closer approach and complete burial of these two residues is hindered by the bulkier side chains of M7 and M7′ and the steric hindrance and charge repulsion presented by K5 and K5′.

The three-dimensional coordinates of human Ca^{2+}-S100B (*14*), rat Ca^{2+}-S100B (*15*), rat apo-S100B (*16*), bovine Ca^{2+}-S100B (*17*), bovine apo-S100B (*18*), rabbit Ca^{2+}-S100A6 (*19*), rabbit apo-S100A6 (*20*), bovine Ca^{2+}-calbindin D_{9k} (*21*), and bovine apo-calbindin D_{9k} (*22*) were used to calculate the accessible surface area (ASA) for each protein. Table 1 shows that the dimer interface ASA values range from 1110 to 1620 Å^2. The interface ASA values of 1400−1500 Å^2 for rat and bovine apo-S100B are above the average of about 900 Å^2 expected for a homodimer of similar size (*29*). The relatively high planarity values of 4.3−5.6 Å indicate the monomers are wrapped around each other, consistent with a high dimerization propensity (*29*). The reported average planarity values of a set of 32 nonhomologous homodimers is 3.46 Å, whereas heterodimers have flatter interfaces with an average planarity value of 2.80 Å

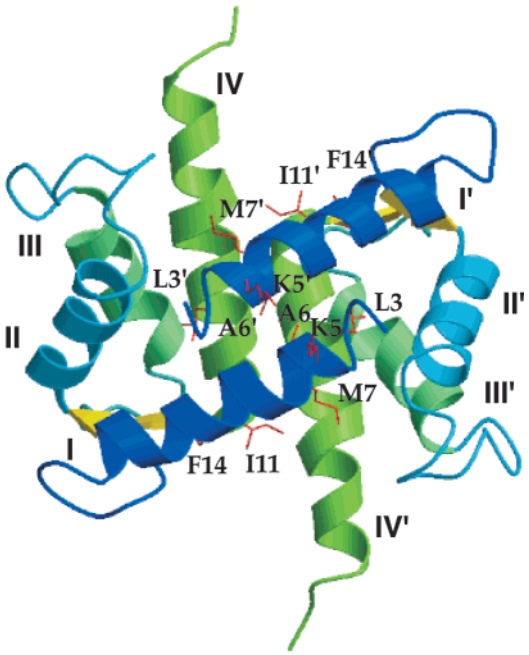

FIGURE 1: Ribbon drawing of the human Ca^{2+}-S100B dimer. The structure is an average of the ensemble of 20 conformers submitted as PDB file code 1uwo (*21*). The residues described in this study are indicated by red stick representations of their side chains. Helices I, IV and I′, IV′ are labeled on their respective monomers.

(*29*). The listed apo-S100 proteins have oblong dimer interfaces (circularity values of 0.64−0.80) that become more circular upon binding calcium (circularity values of 0.75−0.93). The gap volume index of each construct is less than or only slightly above the mean value of 2.20 Å reported for homodimers (*29*). In both rat S100B and rabbit S100A6, for which the gap volume index was measured for apo and calcium-bound forms, the increase in the index in the calcium-bound state suggests the dimer interface becomes less tightly packed. The low gap index values of S100A6 indicate that its dimerization propensity might be particularly high. Nevertheless, while calcium binding results in a significant reorientation of helix III, it is accompanied by <15% reduction in the dimer interface ASA (Table 1), indicating that the dimer scaffold is essentially maintained upon binding calcium. The percentage of polar residues at the dimer interface is not very different from the generally observed composition of polar residues in protein−protein interfaces and protein cores (*30*, *31*).

Despite the numerous S100 structures available, the surface area contribution of individual amino acid residue side chains to the dimer interface has not been previously analyzed. This is shown for Ca^{2+}-S100B in Figure 2A and is representative of the S100 proteins. The dimer interface is formed by helix I (46% of total dimer interface area), helix II (13%), and helix IV (41%). The contribution of helix I to the dimer interface is the focus of the present study because, aside from its large surface area contribution, the changes in interhelical angle between helices I and I′ are relatively minor, whereas helix IV undergoes more significant structural changes when calcium binds (*14*, *18*, *32*). Four residues selected for substitution (L3, M7, I11, and F14) have large side chains that form a hydrophobic face on one side of helix I, as shown in the helical wheel (inset) in Figure 2A. L3 makes the single largest contribution to the dimer interface (12% of the total

[1] Abbreviations: Ca^{2+}-S100B, calcium-saturated S100B; CD, circular dichroism; DLS, dynamic light scatttering; GuHCl, guanidine hydrochloride; ΔG_u, free energy of unfolding in the absence of denaturant; PPI Server, Protein−Protein Interaction Server (www.biochem.ucl.ac.uk/PP/server).

Table 1: Summary of Dimer Interface Properties of S100 Proteins[a]

protein	interface ASA (Å^2)[b]	planarity (Å)[c]	circularity[d]	% polar residues in interface[e]	gap volume index (Å)[f]
human Ca^{2+}-S100B (1uwo)	1110 (17)	4.3	0.93	24	2.38
rat Ca^{2+}-S100B (1qlk)	1200 (16)	4.9	0.75	19	2.59
rat apo-S100B (1b4c)	1400 (20)	5.0	0.64	20	1.99
bovine Ca^{2+}-S100B (1mho)	1340 (22)	4.8	0.89	22	ND
bovine apo-S100B (1cfp)	1540 (25)	4.5	0.71	24	1.15
rabbit Ca^{2+}-S100A6 (1a03)	1540 (24)	5.4	0.93	17	1.19
rabbit apo-S100A6 (2cnp)	1620 (27)	5.6	0.80	26	0.53

[a] The proteins were submitted to the Protein−Protein Interaction Server (www.biochem.ucl.ac.uk/bsm/PP/server/) using the structural coordinates of the listed PDB codes. For most of the NMR-derived coordinate sets, the "most representative" conformer was analyzed by the PPI server. An unpublished average structure of the 20 conformers of PDB code 1uwo was analyzed. The structure coordinates of human apo-S100B have not been determined. Definitions and more detailed explanations of the interface parameters may be found at the PPI Server website and in ref *22*.[b] The listed ASA values are those that each monomer contributes to the dimer interface. Numbers in parentheses indicate the percentage the interface represents of the monomer's total surface area. [c] Planarity is an index measure of the rms deviation of atoms forming the dimer interface from a best-fit plane. The larger the value, the less planar the interface. [d] Circularity is the axial ratio of the dimer interface (i.e., length/breadth). [e] Includes charged and uncharged polar residues. [f] The gap volume index, a measure of the complementarity (tightness of packing) of the dimer interface, is calculated by the PPI Server by dividing the gap volume by the ASA contribution of both monomers to the interface. The Server could not calculate the gap volume index from the structural coordinates of 1mho.

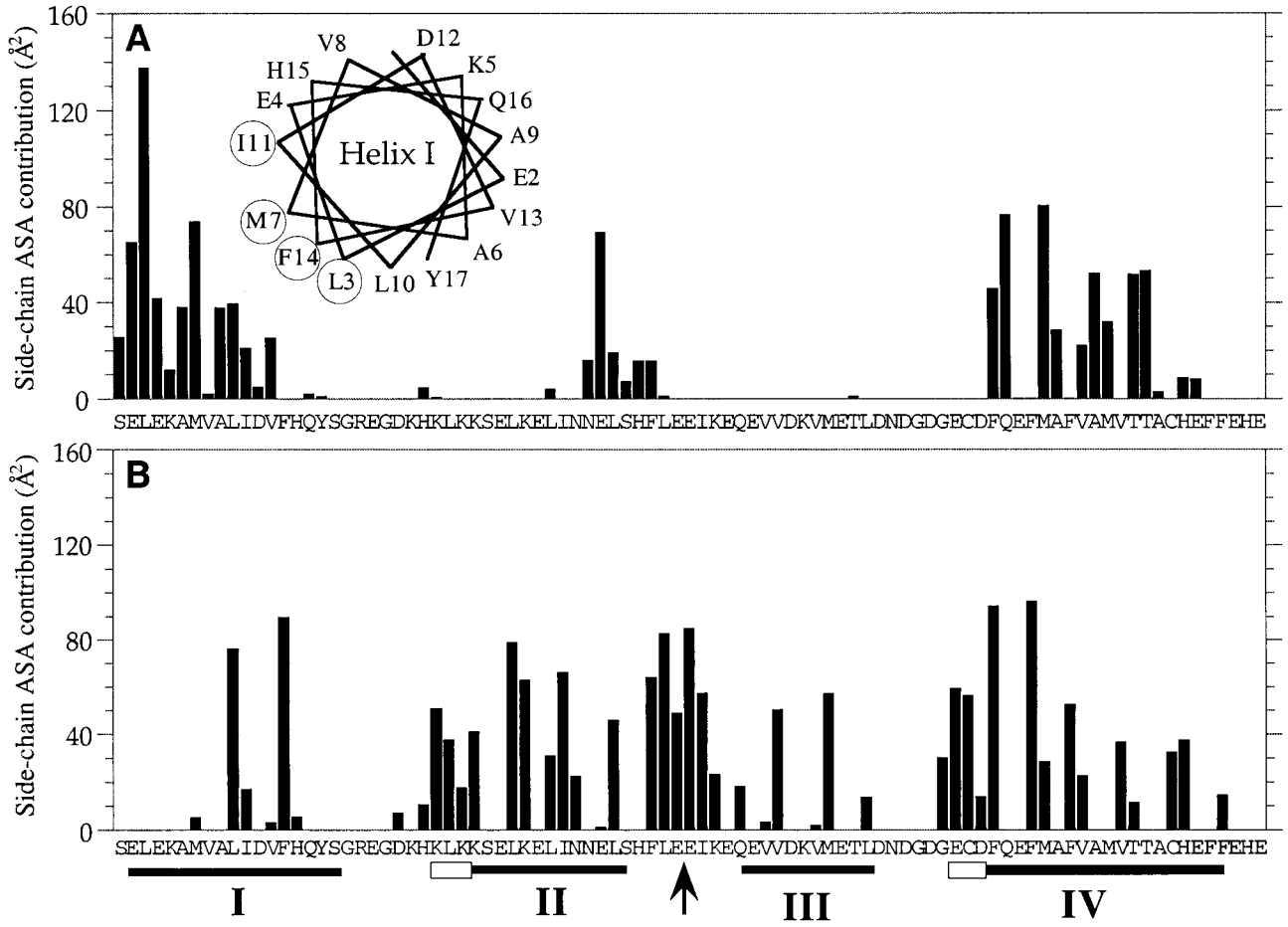

FIGURE 2: (A) Histogram of the ASA contribution of each residue side chain of the human Ca^{2+}-S100B monomer to the dimer interface ASA. The side chain ASA values shown are of the average structure obtained from the 20 conformers of the NMR structure (PDB file code 1uwo). Since chains A and B in each conformer were not constrained to be identical, the average values are of 40 highly representative structures. The residue side chain contributions to the dimer interface were calculated by the Protein−Protein Interaction Server. The secondary structure elements are identified below the protein sequence: α-helix (solid bar) and β-sheet (open box). The helical wheel projection shows that the four residues mutated in this study (circled) form a discrete hydrophobic face in helix I. (B) ASA contribution of each residue side chain to the intramonomeric interface between the N- and C-terminal halves of Ca^{2+}-S100B. Chain A of the average structure was split between Glu45-Glu46 (arrow), and the two halves were submitted to the PPI Server for analysis.

ASA), contributing the equivalent of the entire side chain to the dimer interface (Table 2). Of the remaining helix I residues, M7 makes the next largest contribution to the dimer interface (6.3% of the interface ASA), whereas I11 (1.8%) contributes less, and F14 (0%) appears to make no direct contribution to the dimer interface.

It is well recognized that within the S100 family (including calbindin D_{9k}) the residues corresponding to F14, F70, and

Table 2: Side Chain Surface Area Contributions and Molecular Mass Determination of S100B and Mutants

	buried side chain surface area (Å^2)[a]						
	dimer interface		monomer fold		molecular mass measurements		
protein	apo	Ca	apo	Ca	predicted[b] (Da)	MS[c] (Da)	DLS[d] (kDa)
S100B					21426	ND	28.0 ± 1.6
L3S	110	137	0	0	21374	21374	28.4 ± 1.9
L3A	110	137	0	0	21342	21374	30.5 ± 2.3
M7A	94	73	5	4	21306	21044*	26.1 ± 2.6
I11A	69	21	11	18	21342	21342	24.1 ± 2.2
F14A	28	0	70	90	21272	21272	22.3 ± 3.4
L3A/I11A	179	158	11	18	21258	21258	ND
L3A/F14A	148	137	70	90	21190	21190	ND

[a] The side chain surface areas buried in the dimer interface or in the monomer fold (between N- and C-terminal halves, by the procedure used to generate the data in Figure 2B) for rat apo-S100B (PDB code 1b4c) and human Ca^{2+}-S100B (PDB code 1uwo). [b] The predicted molecular mass of the dimer is based on the nucleotide sequence with the assumption that Met0, which normally is removed, is retained in the overexpressed protein. [c] The mass spectrometry (MS) results are of the predominant species in pure protein preparations which were not uniformly processed to remove the *N*-formyl group or Met0. Typically, >80% of each preparation retained Met0, except for apo-M7A (indicated by an asterisk) in which over half of the preparation had Met0 removed. The mass spectrometry results of the apoproteins are multiplied by 2 to yield the dimer molecular masses listed. [d] Relative molecular masses from dynamic light scattering (DLS) studies of the apoproteins in the absence of denaturant. Molecular mass values were calculated by the Protein Dynamics analysis software using the standard conditions MW curve. The molecular mass values are the means of triplicate readings, with background light scattering subtracted.

F73 in S100B all interact strongly to form the foundation for the hydrophobic core in the monomer (*14*, *33*). To distinguish between inter- and intramonomeric contacts in S100B, the ASA between the N- and C-terminal halves of the protein were analyzed, and the results are shown in Figure 2B. The total interface area between the two helix−loop−helix sites of the protein is 900 Å^2. In contrast to its dimeric fold contribution, L3 makes little contribution to the intramonomeric fold. Likewise, M7 makes only a small contribution to the hydrophobic core of the monomer (5 Å^2) whereas I11 makes nearly the same contribution (18 Å^2) to the intramonomeric fold as to the dimer interface. F14 contributes 90 Å^2 to the monomer core, consistent with its important role in maintaining the calbindin fold (*14*, *33*). Although F14 does not contribute directly to the dimer interface, this residue was selected for mutagenesis to test its effects on monomer structure and the stability of dimerization, particularly since the corresponding residue, F10, in calbindin D_{9k} is one of the hydrophobic core residues that contributes most toward thermodynamic stability (*33*). Furthermore, yeast two-hybrid experiments with human S100P have suggested that the corresponding residue, F15, is directly involved in the dimer interface (*34*). The double mutants L3A/I11A and L3A/F14A were designed to test for cooperative interactions between L3 and either I11 or F14.

Folded State of S100B Mutants. Human S100B is a noncovalent dimer at concentrations >1 μM. However, it is possible that mutations made at the dimer interface (L3A, L3S, M7A, I11A) or integral to the monomer fold (I11A, F14A) could disrupt dimerization. To determine the oligomeric nature of each S100B protein, the mutants were assessed by dynamic light scattering experiments in the absence of calcium. The almost spherical shape of the S100B dimer (54 Å × 51 Å × 41 Å) (14) should make it well suited for this approach. As shown in Table 2, the apparent molecular masses for S100B and the substitution mutants are close to those expected for dimers. The apparent molecular mass values derived from DLS are very similar for S100B, L3A, and L3S but are a little higher than expected, whereas there is a trend of decreasing apparent molecular mass values going from M7A to I11A to F14A.

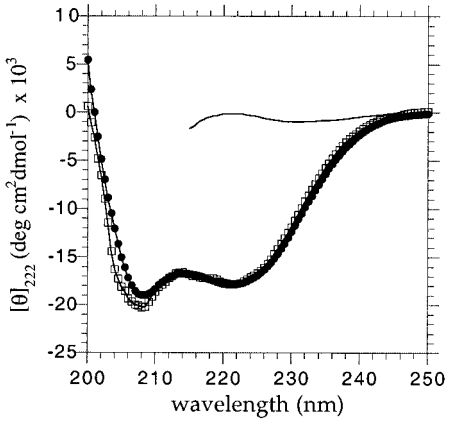

FIGURE 3: CD spectra of the apo forms of S100B (●) and F14A (□). For clarity, the CD spectra of the other mutants are not shown, but their curves are similar to those shown and lie between the apo-S100B and apo-F14A curves. The solid line is apo-S100B in the presence of 7 M GuHCl.

The molecular masses for the L3A and L3S proteins were measured by sedimentation equilibrium analysis, where similar concentrations of protein yielded values of 21.4 ± 0.5 and 21.1 ± 1.0 kDa, respectively, confirming the dimeric state of these proteins (data not shown) and indicating that the DLS technique tends to yield higher than expected molecular mass estimates for these proteins.

Mechanism of Unfolding of Mutant Apo-S100B Proteins. Circular dichroism spectra of some of the apo-S100B mutants studied are shown in Figure 3. All spectra displayed minima at θ_{208} and θ_{222}, which is typical of a largely α-helical fold and consistent with the three-dimensional structures of several S100 proteins (*14*−*22*). The difference in θ_{222} for the substitution mutants is negligible, suggesting that replacement by alanine, a strong helix-forming residue, makes little difference in the α-helical content or helix interactions within this group of proteins. In the presence of 7 M GuHCl the CD spectra of apo-S100B and its mutants show θ_{222} values close to zero (Figure 3). This observation indicates that the protein is denatured and has minimal α-helical structure remaining. Similar results have been obtained for other calcium-binding proteins in the presence of high

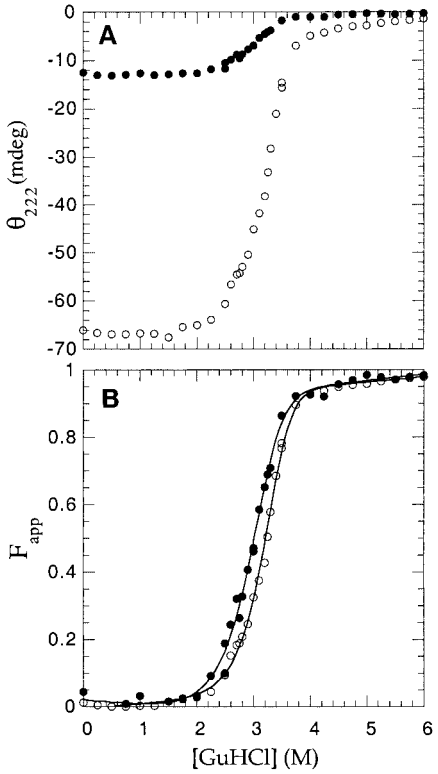

FIGURE 4: GuHCl-induced denaturation curves of apo-S100B at 18.4 μM dimer (○) and 3.7 μM dimer (●). (A) Plot of measured ellipticity values of the proteins as a function of the GuHCl concentration. (B) Plot of the fraction unfolded, F_{app}, of apo-S100B as a function of GuHCl concentration. F_{app} was calculated using eq 2 as described in Materials and Methods. Fitting of these data yielded midpoints of 3.20 ± 0.01 M (○) and 3.00 ± 0.01 M (●).

concentrations of chemical denaturant (*26*, *33*, *35*, *36*).

Unfolding of dimeric proteins by chemical denaturant methods is usually depicted as a three-step process (eq 4) whereby the folded dimer (F_2) dissociates to form a folded monomer (F), followed by production of an unfolded monomer (U). Dynamic light scattering and sedimentation

$$F_2 \overset{K_1}{\rightleftharpoons} 2F \overset{K_2}{\rightleftharpoons} 2U \qquad (4)$$

equilibrium experiments of apo-S100B and the mutant proteins indicate that they are in the folded dimeric state (F_2). In the presence of GuHCl the proteins exhibited CD spectra characteristic of the unfolded monomeric state (U). GuHCl-induced denaturation of the apo-S100B proteins was monitored using θ_{222} as a measure of folded and unfolded protein present. Figure 4A shows a representative chemical denaturation profile for apo-S100B over a range of GuHCl concentrations. As the GuHCl concentration increases, the protein exhibits a single transition from the folded dimer to the unfolded monomer. Chemical denaturation of the S100 proteins is completely reversible since profiles of freshly denatured proteins are indistinguishable from those where the denatured protein was dialyzed to remove GuHCl, reconcentrated, and reanalyzed in a second GuHCl denaturation series (not shown). Further, the denaturation of apo-S100B and all mutants, monitored at differing concentrations of protein, yielded observable differences in the denaturation profiles (Figure 4B). In each case the midpoint for denaturation, C_M, of the lower protein concentration was shifted to

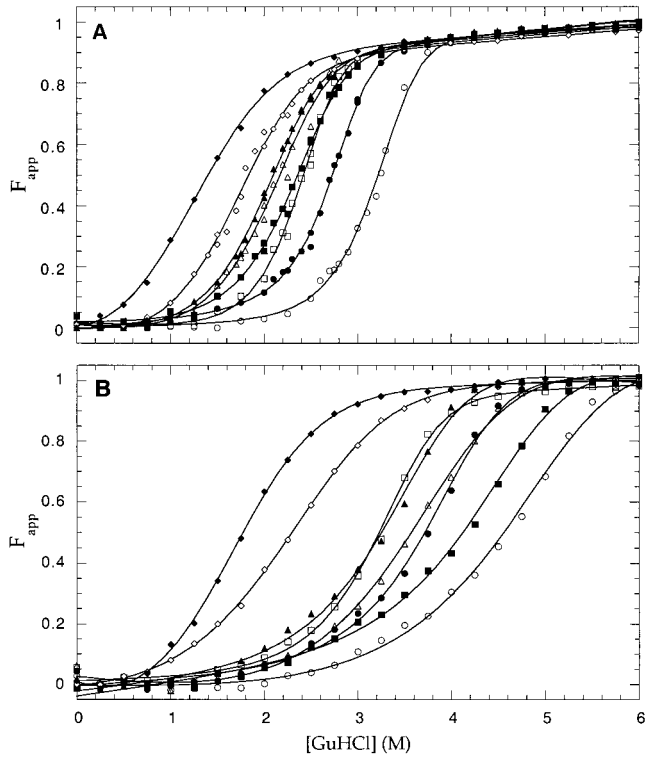

FIGURE 5: GuHCl denaturation profiles of wild-type S100B and its mutants using the background-subtracted CD signal at 222 nm. (A) The apo proteins, with their concentration in dimeric form, are 18.4 μM S100B (○), 18.3 μM L3A (●), 20.7 μM L3S (□), 16.2 μM M7A (△), 16.6 μM I11A (■), 11.2 μM F14A (◇), 14.6 μM L3A/I11A (▲), and 13.6 μM L3A/F14A (◆). (B) The calcium-saturated proteins, with the same symbols as in panel A, have dimer concentrations of 7.3 μM S100B, 11.4 μM L3A, 12.9 μM L3S, 15.3 μM M7A, 13.6 μM I11A, 17.4 μM F14A, 11.9 μM L3A/I11A, and 16.7 μM L3A/F14A.

lower GuHCl concentration. This observation is indicative of a concentration dependence on the unfolding profile. In the case of the S100 proteins studied here it shows that the reaction is bimolecular and cannot result from the unfolding of a folded monomer (F) to its unfolded state only. The smooth transition observed during the unfolding reaction therefore shows no evidence of a folded monomeric intermediate (F). This approach, which is similar to that used for the unfolding of other dimeric proteins (*27*, *28*), was simplified to a two-state process (eq 5), where K_u is the unfolding equilibrium constant.

$$F_2 \overset{K_u}{\rightleftharpoons} 2U \qquad (5)$$

The unfolding profiles of apo-S100B and the mutants are shown in Figure 5A. In each case a smooth transition for unfolding was obtained. The data show that the midpoints of the curves, C_M, range from about 3.2 M for apo-S100B to near 1.3 M for the L3A/F14A mutant. By visual inspection, the apparent order of stability of the mutants is apo-S100B > L3A > L3S > I11A > M7A ∼ L3A/I11A > F14A > L3A/F14A. For quantitative comparison of the stabilities, the CD data in Figure 5A were analyzed in terms of ΔG_u, the free energy of unfolding, and m_D, the dependence of ΔG_u on the denaturant concentration. The results are shown in Table 3.

In the absence of calcium, wild-type S100B is the most resistant to denaturation, as expected. However, a wide range

Table 3: Free Energies of Unfolding for Apo and Ca Forms of S100B and Its Mutants

	apo				calcium saturated		
protein	m_D[a] (kJ mol^{-1} M^{-1})	C_M[b] (M GuHCl)	ΔG_u[c] (kJ mol^{-1})	$\Delta\Delta G_u$[d] (kJ mol^{-1})	m_D[a] (kJ mol^{-1} M^{-1})	C_M[b] (M GuHCl)	$\Delta\Delta G_u$[d] (kJ mol^{-1})
S100B	-13.9 ± 1.3	3.2	72.4 ± 4.0	0.0	-4.4 ± 1.0	4.6	0.0
L3A	-14.6 ± 1.6	2.7	67.4 ± 4.6	-5.0	-6.6 ± 1.3	3.7	2.2
L3S	-13.8 ± 1.3	2.4	60.8 ± 3.7	-11.6	-9.6 ± 1.2	3.2	8.0
M7A	-10.8 ± 2.8	2.2	50.4 ± 6.6	-22.0	-5.7 ± 0.7	3.6	-2.7
I11A	-11.5 ± 1.2	2.3	55.2 ± 2.9	-17.3	-6.0 ± 1.0	4.2	4.5
F14A	-8.1 ± 1.5	1.8	40.9 ± 3.5	-31.5	-4.5 ± 0.6	2.3	-14.3
L3A/I11A	-11.9 ± 1.6	2.1	51.1 ± 3.6	-21.3	-7.4 ± 1.7	3.3	3.2
L3A/F14A	-7.0 ± 1.2	1.3	35.1 ± 2.7	-37.4	-3.4 ± 1.2	1.7	-21.6

[a] The slope, m_D, is a measure of the cooperativity of the unfolding reactions. [b] C_M, the concentration of GuHCl at which the protein is 50% unfolded. [c] The Gibbs free energy of unfolding in the absence of denaturant. The ΔG_u value is not calculated for the calcium-saturated proteins, for reasons discussed in the text. [d] $\Delta\Delta G_u$, the difference in stability of the apo or calcium-saturated form of the protein compared to the apo-S100B or Ca^{2+}-S100B protein, where $\Delta\Delta G_u = \Delta G_u^{mut} - \Delta G_u^{wt}$.

of stabilities was observed from 72.4 kJ mol^{-1} for the wild-type protein to 35.1 kJ mol^{-1} for the L3A/F14A double mutant. Whereas all sites of mutation tested the effects of replacement by alanine, a serine replacement was also tested at position L3. The L3S mutant protein shows a significantly reduced stability relative to the parent ($\Delta\Delta G_u = -11.6$ kJ mol^{-1}) and compared to L3A (-6.6 kJ mol^{-1}). The $\Delta\Delta G_u$ values of the two double mutations are close to the additive values of the individual mutations, suggesting there is no cooperative effect between the L3A mutation and either the I11A or the F14A mutation. The slopes of denaturation curves, m_D, vary by more than 2-fold from 14.6 kJ mol^{-1} M^{-1} for L3A mutant to 7.0 mol^{-1} M^{-1} for the L3A/F14A double mutant. Similar differences in slopes have been observed in mutational analysis of apo-calbindin D_{9k} (*33*).

Stability of Calcium-Saturated S100B Mutant Proteins. The stability of the S100B proteins was also assessed in the presence of a large excess of calcium. As with the apo proteins, the unfolding of the calcium form can be approximated as a two-state transition, as shown in eq 6. Since

$$F_2Ca_4 \overset{K_u^{Ca}}{\rightleftharpoons} 2U + 4Ca \qquad (6)$$

the reported calcium dissociation constants for S100B are between 10 and 50 μM (*9*), a 400-fold molar excess of calcium was used to ensure that the F_2Ca_4 species was the only calcium-bound species populated during the unfolding reaction. This allows the unfolding of the mutant proteins to be studied with respect to the parent protein ($\Delta\Delta G_u$). However, direct quantitative comparison of ΔG_u with the apo forms is not feasible since the total calcium concentration [Ca_t] influences the calculation of the absolute value of ΔG_u.

It general, the unfolding profiles for the calcium-bound proteins were shifted to higher GuHCl concentrations (Figure 5B), consistent with an increased stability of the calcium forms of the protein with respect to the apo proteins. This is reflected in the general trend of higher midpoints for denaturation. For example, the C_M for S100B increased by 1.4 M GuHCl upon addition of calcium. However, smaller changes were observed for other mutants. The results shown in Table 3 indicate that, unlike the apo proteins, there are mutant proteins with increased stability, whereas others have decreased stability compared to the wild-type protein. In particular, the mutants L3S, L3A, I11A, and L3A/I11A are more stable than wild-type S100B by as much as 8 kJ mol^{-1}. Similar to their apo forms, the least stable species are F14A and L3A/F14A, although the effects were not as dramatic. For example, L3A/F14A is less stable compared to the wild type by 37.4 kJ mol^{-1} in the apo state and by 21.6 kJ mol^{-1} in the calcium-bound form. In contrast to the additive effects observed in the apo states, the double mutants L3A/I11A and L3A/F14A exhibit $\Delta\Delta G_u$ values either intermediate or significantly greater than predicted, based on the two single mutants. For example, $\Delta\Delta G_u$ for L3A (2.2 kJ mol^{-1}) and I11A (4.5 kJ mol^{-1}) lie on either side of the $\Delta\Delta G_u$ observed for the L3A/I11A mutant (3.2 kJ mol^{-1}). However, it is clear that the general stabilizing abilities of these mutations are maintained. Conversely, the decrease in stability of the L3A/F14A mutation ($\Delta\Delta G_u = -21.6$ kJ mol^{-1}) is significantly greater than expected for the additive effects of the destabilizing F14A mutation (-14.3 kJ mol^{-1}) and the weakly stabilizing L3A mutation (2.2 kJ mol^{-1}). This trend is more difficult to reconcile but indicates that the destabilizing ability of F14A is the more dominant property in the protein.

The slopes of the unfolding curves for the calcium-bound protein varied from 9.6 kJ mol^{-1} M^{-1} for the L3S mutant to 3.4 kJ mol^{-1} M^{-1} for L3A/F14A. In general, these values are significantly lower than observed for the apo proteins but are similar to slopes obtained for unfolding of other proteins in the calcium-bound state (*26*) and are consistent with the greater stability of calcium-saturated EF-hand proteins (*33*, *36*).

DISCUSSION

Site-directed mutagenesis studies have been used extensively to study EF-hand calcium-binding proteins such as calmodulin, troponin C, and calbindin D_{9k}. Several studies have analyzed the impact of mutations to specific residues at the calcium-ligating positions in the calcium-binding loop on the calcium affinity, structure, and stability of these proteins. For example, it has been observed that replacement of the acidic ligating residues in site III of troponin C (*37*, *38*), sites I and II of calbindin D_{9k} (*39*), and parvalbumin (*40*) can decrease calcium affinity by more than 100-fold. An EF-hand is more than just its Ca^{2+}-binding loop, since the flanking helices in the EF-hand can also have a dramatic effect on calcium affinity, as has been demonstrated by mutational analyses of these helices (*12*, *41*). Elegant studies by Kragelund et al. (*13*) and Julenius et al. (*33*) show that residues comprising the hydrophobic core of calbindin D_{9k}

also have significant effects on calcium affinity even though these residues can be far removed from the calcium-binding loops. The current work takes a first look at the importance of hydrophobic residues toward the stability of the calcium-binding protein S100B. Unlike calbindin D_{9k}, S100B is dimeric, and the current work examines residues at both the dimer interface and the hydrophobic core of the constituent monomers.

Thermodynamic Stability of Human S100B. The stability of human apo-S100B was measured by GuHCl denaturation in the present study, yielding a ΔG_u of 72.4 kJ mol^{-1}. This value is significantly higher than the 20−60 kJ mol^{-1} range typically observed for soluble monomeric proteins (*42*) and is greater than the stability of other EF-hand calcium-binding proteins such as troponin C and calmodulin (*26*, *35*, *36*) in which intact proteins or EF-hand domains have ΔG_u values ranging from 8 to 65 kJ mol^{-1}. Furthermore, the ΔG_u for apo-S100B is more than twice that of its monomeric relative apo-calbindin D_{9k} (27 kJ mol^{-1}) determined by urea denaturation (*33*). A portion of this difference may be attributable to the use of different denaturants between the studies. In support of this, two reports show that the ΔG_u obtained by GuHCl denaturation of calcium-binding proteins is higher than that obtained by urea unfolding (*35*, *36*). However, apo-S100B is resistant to complete unfolding by urea (data not shown), precluding this comparison. The higher stability of apo-S100B compared to calbindin D_{9k} likely results from a greater buried hydrophobic surface area at both its dimer interface and the hydrophobic core of its constituent monomers. Apo-S100B has about 1400−1500 Å^2 of buried surface area from hydrophobic residues at the dimer interface (Table 1) and another 900 Å^2 buried by each monomeric half subunit as the N- and C-terminal EF-hands pack against each other. This latter value is similar to the buried surface area of 990 Å^2 for the interface between EF-hands 1 and 2 of calbindin D_{9k} (*43*). Both proteins have similar buried surface area within each EF-hand. Thus, the dimer interface accounts for much of the difference in buried hydrophobic core residues between S100B and calbindin D_{9k}. This more extensive hydrophobic core in S100B and the resultant increased stability are consistent with the evolution of oligomeric proteins, which are generally more stable than their monomeric counterparts (*44*).

Dimer vs Monomer Stabilizing Residues. Analysis of the dimer interface for S100B shows an extensive network of hydrophobic interactions along helix I (L3, A6, M7, L10, I11). It seemed logical to use the burial of hydrophobic side chains as the criterion for selection of amino residues to mutate in order to probe this interface. This might be expected to disrupt the dimer, perhaps leading to either folded or unfolded monomeric units. However, dynamic light scattering and sedimentation equilibrium experiments indicate that none of the mutations lead to any observable formation of the monomeric protein at the concentrations studied. Further, all mutant proteins are α-helical with nearly identical magnitudes of θ_{208} and θ_{222}. Since the magnitude of the ellipticity at these wavelengths is sensitive to helix−helix interactions (*41*), this similarity indicates that the X-bundle structure of the proteins is preserved.

Mutation to residues of helix I of apo-S100B leads to decreased stability compared to the parent protein, similar to observations for calbindin D_{9k} where mutations to residues L6 and F10 in the analogous helix result in decreased stability (*33*). The values of $\Delta\Delta G_u$ for the single site mutations (L3A, L3S, M7A, I11A, and F14A) range from −5.0 (for L3A) to −31.5 kJ mol^{-1} (for F14A). For apo-S100B these observations are also additive since the double mutations studied (L3A/I11A, L3A/F14A) have $\Delta\Delta G_u$ values near the sum of the individual mutations, indicating that these mutations do not act synergistically to destabilize the protein. This is consistent with the three-dimensional structures of S100 proteins that show there is little or no interaction between residues corresponding to L3, I11, and F14 in the structures (*14*−*22*).

On the basis of dimer surface area, L3 is nearly completely buried and makes the largest ASA contribution to the dimer interface. However, the L3A or L3S mutations have the smallest observed effects on the stability, −5.0 and −11.6 kJ mol^{-1}, respectively. In a tightly packed interior with no solvent accessibility, a Leu to Ala substitution results in a $\Delta\Delta G_u$ of about -19 ± 8 kJ mol^{-1} in barnase (*45*), a value that is close to observed stability decreases of Leu to Ala substitutions in the core of calbindin D_{9k} (*33*). However, the effects on the hydrophobic core (and ultimately on the stability of the protein) of reducing the side chain surface area of a residue by mutation depend on the whether the core is rigidly packed or has some side chain mobility allowed (*45*−*47*) and whether the side chain is completely buried or partially solvent accessible (*47*). An explanation for the small changes in $\Delta\Delta G_u$ for L3A and L3S is provided by the I3A mutation in T4 lysozyme in which a similar sized side chain reduction leads to only a 3 kJ mol^{-1} decrease in $\Delta\Delta G_u$ (*47*). The small decrease in stability is a result of the increased dynamics of residues near the amino terminus of the helix and partial solvent accessibility of the side chain, particularly since it is near the periphery of the hydrophobic core of lysozyme. A similar effect is likely occurring in apo-S100B for the L3A mutation. In support of this, ^{15}N relaxation experiments show little mobility of the backbone (*48*) while amide exchange experiments (unpublished data) indicate that this region is more exposed to solvent that other helical sections in S100B. Consistent with this interpretation, sequence alignment of S100 proteins shows that shorter side chain residues such as Ala, Thr, and Met are also found at position 3. Together these indicate that, despite its apparent burial in S100B, Leu3 is not a critical residue for dimer maintenance.

The largest single effect on the stability of apo-S100B results from the F14A mutation in which ΔG_u decreases by nearly 32 kJ mol^{-1}. Despite the >40% decrease in stability, the F14A protein is able to dimerize. The $\Delta\Delta G_u$ of F14A is very similar to results for the corresponding mutation (F10A) in calbindin D_{9k} where a decrease in stability of about 20 kJ mol^{-1} is noted. In calbindin D_{9k} F10, F63, and F66 form a hydrophobic triad that is key to the protein's stability. In S100B the corresponding residues, F14, F70, and F73, are also closely packed (*14*). It is interesting that the decrease in stability for F14A in S100B is nearly twice that of F10A in calbindin D_{9k}. This likely occurs because $\Delta\Delta G_u$ in S100B results from the sum of the two F14A positions (one in each monomer) in the protein, both of which are nearly completely buried in the monomeric fold. Further, the denaturation slopes of the F14A (S100B) and F10A (calbindin D_{9k}) mutations are reduced by about 40% compared to the wild-type

proteins. These similarities indicate that F14 in S100B and F10 in calbindin D_{9k} have common roles in the folding pathways and maintenance of the monomeric fold. This conclusion is in contrast to yeast two-hybrid studies of human S100P (*34*) which indicated that F15 (F14 in S100B) is a critical residue for dimer maintenance. The current work indicates that F14 has a dominant role in the $2U \rightleftarrows 2F$ equilibrium step (eq 4) which in turn could compromise dimer formation.

In S100B, M7 makes the fourth largest ASA contribution to the dimer interface and resides close to the crossover point of helices I and I′. Correspondingly, the M7A mutant is largely destabilized (-22 kJ mol^{-1}) compared to the parent protein. This would translate into an increase in K_d of 8000-fold if this decrease in stability arises strictly from a destabilization of the dimer. On the basis of an estimate for a dimerization constant of <0.5 nM for rat apo-S100B (*49*), this would indicate that the M7A mutant has a K_d <4.0 μM. However, neither dynamic light scattering analysis of 16 μM apo-M7A (Table 2) nor the results of the GuHCl denaturation of 3.2 μM apo-M7A (not shown) show the presence of monomers. This would indicate that the K_d for apo-S100B must be at least 10-fold lower (i.e., 0.05 nM) than previously suggested (*49*).

The apo forms of S100B and its mutations in helix I show a strong correlation between ΔG_u and buried surface area. With the exception of L3A and L3S, $\Delta\Delta G_u$ is smallest for I11A, which has the smallest buried surface area contribution, and increases systematically toward L3A/F14A, which has the largest buried surface area contribution. In the calcium-bound states, this trend is less evident although mutations involving F14 clearly destabilize the protein to the greatest extent. An interesting observation is the increased stability ($\Delta\Delta G_u = 4.5$ kJ mol^{-1}) of the I11A mutant compared to S100B in the calcium-bound state. This likely occurs from the 50% decrease of buried surface area of this residue upon calcium binding (Table 2) and concomitant increase in exposure of this side chain to solvent. As a result, the replacement of the Ile residue with Ala would result in a more favorable solvated form of the protein in the calcium-bound state. The increased stability of the calcium forms of L3A and L3S compared to S100B is also suggestive of greater exposure of L3 in the calcium-bound state and subsequent stablization through use of a smaller side chain (Ala) or a hydrophilic one (Ser). However, the small apparent increase in buried surface area of L3 upon calcium binding (Table 2) would appear to contradict this possibility.

Cooperativity of Unfolding. In the calcium-saturated state, the unfolding of S100B and each of its mutants has slopes (m_D) that decrease between 1.4- and 3-fold compared to their respective apo forms. This indicates that unfolding of the calcium-bound state is less cooperative than that of the apo state and likely results from the addition of at least one extra step in the unfolding reactions, namely, the removal of the coordinated calcium ions. The differences in slopes among the proteins in the apo state are more pronounced than those in the calcium-bound state and parallel observations for the order of stability of the mutant proteins in the apo state (Table 3). In support of this, the relationship between $\Delta\Delta G_u$ and the change in slopes (Δm) among the apo forms of the proteins is shown in Figure 6. There is a strong correlation between cooperativity and $\Delta\Delta G_u$. This observation is in contrast to previous studies with calbindin D_{9k} and other proteins (*33*) where a correlation between $\Delta\Delta G_u$ and Δm was not apparent. It is interesting to note that the current work focuses on a small set of mutants localized to one region (helix I) of S100B whereas the other studies have used a broad cross section of mutants distributed throughout an entire protein. Therefore, the strong correlation in Figure 6 may be a good indication of local unfolding rather than global unfolding cooperativity. Further, in Figure 6 there is a large gap between the M7A and F14A points. This occurs between a residue fully involved in the dimer contact (M7) and one wholly involved in the monomer fold (F14). It is tempting to suggest that this large difference reflects a change in the cooperativity of folding for the dimer compared to the monomer. Further data will be required to strengthen this hypothesis.

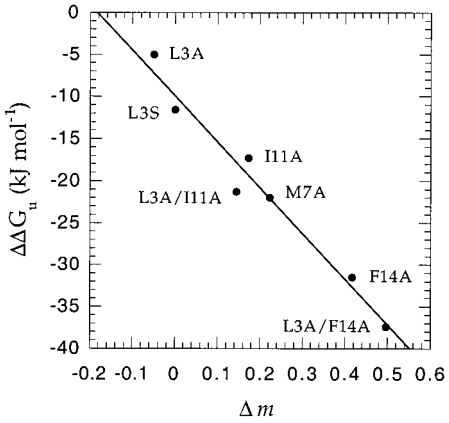

FIGURE 6: Difference in free energy of unfolding ($\Delta\Delta G_u$) as a function of the relative difference in cooperativity of unfolding, Δm, of apo-S100B and mutant proteins. The values of Δm were calculated as $(m_{\text{wild type}} - m_{\text{mutant}})/m_{\text{wild type}}$. The best fit line shown has $r = 0.98$.

REFERENCES

1. Ikura, M. (1996) *Trends Biochem. Sci. 21*, 14−17.
2. Zimmer, D. B., Cornwall, E. H., Landar, A., and Song, W. (1995) *Brain Res. Bull. 37*, 417−429.
3. Schäfer, B. W., and Heizmann, C. W. (1996) *Trends Biochem. Sci. 21*, 134−140.
4. Donato, R. (1999) *Biochim. Biophys. Acta 1450*, 191−231.
5. Sheng, J. G., Mrak, R. E., Rovnaghi, C. R., Kozlowska, E., van Eldik, L. J., and Griffin, W. S. T. (1994) *Neurobiol. Aging 17*, 359−363.
6. Marshak, D. R., Pesce, S. A., Stanley, L. C., and Griffin, W. S. T. (1992) *Neurobiol. Aging 13*, 1−7.
7. Griffin, W. S. T., Sheng, J. G., McKenzie, J. E., Royston, M. C., Gentleman, S. M., Brumback, R. A., Cork, L. C., Del Bigio, M. R., Roberts, G. W., and Mrak, R. E. (1998) *Neurobiol. Aging 19*, 401−405.
8. Baudier, J., and Cole, R. D. (1988) *J. Biol. Chem. 263*, 5876−5883.
9. Baudier J., and Cole, R. D. (1989) *Biochem. J. 264*, 79−85.
10. Miwa, N., Kobayashi, M., Takamatsu, K., and Kawamura, S. (1998) *Biochem. Biophys. Res. Commun. 251*, 860−867.
11. Tanaka, T., Miwa, N., Kawamura, S., Sohma, H., Nitta, K., and Matsushima, N. (1999) *Protein Eng. 12*, 395−405.
12. Tsuji, T., and Kaiser, E. T. (1991) *Proteins 9*, 12−22.
13. Kragelund, B. B., Jonsson, M., Bifulco, G., Chazin, W. J., Nilsson, H., Finn, B. E., and Linse, S. (1998) *Biochemistry 37*, 8926−8937.
14. Smith, S. P., and Shaw, G. S. (1998) *Structure 6*, 211−222.
15. Drohat, A. C., Baldisseri, D. M., Rustandi, R. R., and Weber, D. J. (1998) *Biochemistry 37*, 2729−2740.

16. Drohat, A. C., Tjandra, N., Baldisseri, D. M., and Weber, D. J. (1999) *Protein Sci. 8*, 800−809.
17. Matsumura, H., Shiba, T., Inoue, T., Harada, S., and Kai, Y. (1998) *Structure 6*, 233−241.
18. Kilby, P. M., Van Eldik, L. J., and Roberts, G. C. (1996) *Structure 4*, 1041−1052.
19. Sastry, M., Ketchem, R. R., Crescenzi, O., Weber, C., Lubienski, M. J., Hidaka, H., and Chazin, W. J. (1998) *Structure 6*, 223−231.
20. Mäler, L., Potts, B. C. M., and Chazin, W. J. (1999) *J. Biomol. NMR 13*, 233−247.
21. Kordel, J., Skelton, N. J., Akke, M., and Chazin, W. J. (1993) *J. Mol. Biol. 231*, 711−734.
22. Skelton, N. J., Kordel, J., and Chazin, W. J. (1995) *J. Mol. Biol. 249*, 441−462.
23. Dulau, L., Cheyrou, A., and Aigle, M. (1989) *Nucleic Acids Res. 17*, 2873.
24. Smith, S. P., Barber, K. R., Dunn, S. D., and Shaw, G. S. (1996) *Biochemistry 35*, 8805−8814.
25. Cohn, E. J., and Edsall, J. T. (1943) in *Proteins, Amino Acids, and Peptides*, pp 157−161, Reinhold, New York.
26. Shaw, G. S., Hodges, R. S., Kay, C. M., and Sykes, B. D. (1994) *Protein Sci. 3*, 1010−1019.
27. Reece, L. J., Nichols, R., Ogden, R. C., and Howell, E. E. (1991) *Biochemistry 30*, 10895−10904.
28. Mann, C. J., and Matthews, C. R. (1993) *Biochemistry 32*, 5282−5290.
29. Jones, S., and Thornton, J. M. (1996) *Proc. Natl. Acad. Sci. U.S.A. 93*, 13−20.
30. Miller, S., Janin, J., Lesk, A. M., and Chothia, C. (1987) *J. Mol. Biol. 196*, 641−656.
31. Kajander, T., Kahn, P. C., Passila, S. H., Cohen, D. C., Lehtiö, L., Adolfsen, W., Warwicker, J., Schell, U., and Goldman, A. (2000) *Structure 8*, 1203−1214.
32. Drohat, A. C., Amburgey, J. C., Abildgaard, F., Starich, M. R., Baldisseri, D., and Weber, D. J. (1996) *Biochemistry 35*, 11577−11588.
33. Julenius, K., Thulin, E., Linse, S., and Finn, B. E. (1998) *Biochemistry 37*, 8915−8925.
34. Koltzscher, M., and Gerke, V. (2000) *Biochemistry 39*, 9533−9539.
35. Fredricksen, R. S., and Swenson, C. A. (1996) *Biochemistry 35*, 14012−14026.
36. Masino, L., Martin, S. R., and Bayley, P. M. (2000) *Protein Sci. 9*, 1519−1529.
37. Marsden, B. J., Hodges, R. S., and Sykes, B. D. (1988) *Biochemistry 27*, 4198−4206.
38. Marsden, B. J., Shaw, G. S., and Sykes, B. D. (1990) *Biochem. Cell. Biol. 68*, 587−601.
39. Linse, S., Brodin, P., Drakenberg, T., Thulin, E., Sellers, P., Elmden, K., Grundstrom, T., and Forsen, S. (1987) *Biochemistry 26*, 6723−6735.
40. Cates, M. S., Berry, M. B., Ho, E. L., Li, Q., Potter, J. D., and Phillips, G. N., Jr. (1999) *Structure 7*, 1269−1278.
41. Monera, O. D., Shaw, G. S., Zhu, B.-Y., Sykes, B. D., Kay, C. M., and Hodges, R. S. (1992) *Protein Sci. 1*, 945−955.
42. Makhatadze, G. I., and Privalov, P. L. (1995) *Adv. Protein Chem. 47*, 307−425.
43. Håkansson, M., Svensson, A., Fast, J., and Linse, S. (2001) *Protein Sci. 10*, 927−933.
44. Jaenicke, R., and Lilie, H. (2000) *Adv. Protein Chem. 53*, 329−401.
45. Serrano, L., Kellis, J. T., Jr., Cann, P., Matouschek, A., and Fersht, A. R. (1992) *J. Mol. Biol. 224*, 783−804.
46. Kellis, J. T., Jr., Nyberg, K., and Fersht, A. R. (1989) *Biochemistry 28*, 4914−4922.
47. Matsumura, M., Becktel, W. J., and Matthews, B. W. (1988) *Nature 334*, 406−410.
48. Inman, K. G., Baldisseri, D. M., Miller, K. E., and Weber, D. J. (2001) *Biochemistry 40*, 3439−3448.
49. Drohat, A. C., Nenortas, E., Beckett, D., and Weber, D. J. (1997) *Protein Sci. 6*, 1577−1582.

BI0118052